Macromolecules

Article

Cite This: Macromolecules 2019, 52, 9389−9397

pubs.acs.org/Macromolecules

Impact of Cyclic Block Copolymer Chain Architecture and Degree of Polymerization on Nanoscale Domain Spacing: A Simulation and Scaling Theory Analysis

Amy D. Goodson, Jessie E. Troxler, Maxwell S. Rick, Henry S. Ashbaugh,* and Julie N. L. Albert*

Department of Chemical and Biomolecular Engineering, Tulane University, New Orleans, Louisiana 70118, United States

Supporting Information

ABSTRACT: Cyclic block copolymers are predicted to assemble into nanostructured domains up to 40% smaller than their linear analogues, making them promising alternatives for nanoscale patterning applications. The limited cyclic block copolymer structures observed experimentally, however, have not met the domain reductions predicted by scaling theory. Through a systematic dissipative particle dynamics simulation study of linear and cyclic block copolymer assembly into lamellar and cylindrical nanostructures, we explore these discrepancies. We find standard implementations of scaling theory, which assume a cyclic BCP behaves as a linear molecule of half the contour length, fail to account for finite chain size effects, resulting in overpredictions of the extent of domain shrinkage upon cyclization. We propose a revised scaling law that clarifies the interplay of chain length, segregation strength, and chain architecture in determining domain spacing reduction attainable by molecular cyclization and offers an explanation for the discrepancies between prior theoretical predictions and experimental results.

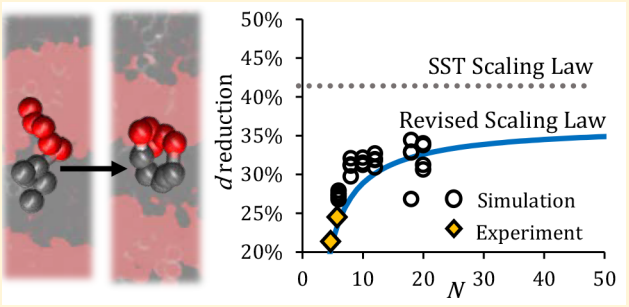

1. INTRODUCTION

Advancements in photolithography to produce increasingly finer features have spurred an exponential growth in computing power over the past 50 years, doubling the number of transistors on silicon wafers approximately every 18 months. Realizing features 10 nm or smaller by photolithography, however, is prohibitively expensive due to the need for high-powered, extreme ultraviolet light sources[1] with superior resolution to circumvent the diffraction limit of light.[2] Nanopatterning by block copolymers (BCPs), which form nanoscale assemblies with dimensions dictated by polymer molecular weights, chemistry, and architecture, offers an attractive, potentially lower cost alternative to photolithography.

BCPs consist of two or more covalently bound chemically distinct homopolymer blocks. Thermodynamic incompatibility between blocks drives phase separation; however, the covalent linkages limit segregation to the nanometer scale. As a result, BCPs self-assemble into a variety of nanoscale morphologies that minimize the free energy under the constraints imposed by the polymer's chemical composition and topology.[3,4] Generally, the equilibrium diblock copolymer (i.e., *AB* BCP where *A* and *B* refer to the two blocks) self-assembled nanostructure is dictated by the volume fraction of the *A* block ($f_A = 1 - f_B$) and the segregation strength (χN, the product of the Flory−Huggins interaction parameter, χ, and the BCP degree of polymerization, N). Symmetric linear BCPs ($f_A = f_B = 0.5$) form lamellar structures above the order−disorder transition ($\chi N|_{\mathrm{lin}}^{\mathrm{ODT}} \approx 10.5$), while asymmetric linear BCPs ($f_A \neq f_B$) can form hexagonally packed cylinders (HPC), spheres, or bicontinuous structures. Significant research has focused on the use of the lamellar and cylindrical BCP morphologies for "bottom-up" nanolithography, although commercial applications have been limited. The ability to reliably pattern large scale, defect-free, sub-10 nm features would significantly advance BCP nanolithography, meeting the microelectronics industry's needs for improved pattern resolution.

Linear BCP feature sizes depend most strongly on N, which controls the overall polymer size, and weakly on χ, which characterizes the degree of incompatibility between the different blocks. Thus, the most direct approach to reducing linear BCP domain spacing has been to synthesize shorter chains. High χ systems allow for shorter chains to maintain order, but the large surface energy difference between blocks introduces additional challenges for BCP synthesis and assembly.[5−8] Use of multiblock and nonlinear BCP architectures is a promising paradigm for overcoming these challenges. For example, both linear *ABA* triblock and $(AB)_x$ star copolymers form smaller ordered domains[9−15] at lower χN[13,16,17] with narrower interfaces[18] than their *AB* counterparts.

Received: September 24, 2019
Revised: November 7, 2019
Published: November 27, 2019

DOI: 10.1021/acs.macromol.9b02015
Macromolecules 2019, 52, 9389−9397

Cyclic BCPs are expected to form domains significantly smaller than their linear analogues while exhibiting superior thin film stability[19] and assembly dynamics.[20−22] Theory,[23,24] simulation predictions,[25−27] and experimental observations[28,29] have all found that the phase diagram of cyclic BCPs resembles the linear phase diagram with the ODT shifted to a slightly higher segregation strength ($\chi N|_{cyc}^{ODT} \approx 1.7\chi N|_{lin}^{ODT}$), but with smaller nanostructures. Poelma et al., for example, found that cyclic polystyrene-*b*-poly(ethylene oxide) (cyc-(PS-*b*-PEO)) formed cylindrical domains 25% smaller than those of linear BCPs with the same chemistry and degree of polymerization.[30] When they tried to achieve similarly sized domains with a linear BCP of half the molecular weight, the system was disordered. Similarly, Gartner and co-workers showed that cyclizing linear polystyrene-*b*-poly(oligo(ethylene glycol) methacrylate) (PS-*b*-POEGMA) decreased domain spacing by 18−21%.[31] A consensus of theoretical and simulation work suggests that cyclization can decrease diblock copolymer feature sizes up to 40%.[9,23,24,27] However, to our knowledge, no one has systematically explored the relationship between degree of polymerization and intermolecular interactions in determining feature sizes formed by cyclic copolymers.

Semenov's theoretical framework[32−34] has been widely influential for predicting linear BCP feature sizes in the strong segregation regime ($\chi N \gg \chi N|_{lin}^{ODT}$). In this theory, the free energy of the BCP melt is expressed as a linear combination of contributions due to unlike monomer contact at the domain interfaces, which favors domain swelling to minimize interblock contact, and chain stretching, which opposes domain growth that drives chains away from their ideal Gaussian conformations.[33,35] Minimization of the free energy with respect to the domain spacing, d, yields the scaling law

$$d = \beta\chi^{1/6}N^{2/3} \tag{1}$$

where the prefactor β depends on the characteristic segment length and f_A.[4,36] Experiments with lamellar BCPs have confirmed the strong dependence of domain spacing on N with scaling exponents ranging from 0.61 to 0.64,[37,38] but to our knowledge, this relationship has not been tested for asymmetric BCPs. The weaker χ dependence has proven challenging to study experimentally but has been verified by simulation.[31,39] Additionally, the derivation of strong segregation theory (SST) assumes the polymers are very long ($\chi N \to \infty$) which may limit its applicability for lithography, where N is minimized to shrink feature sizes. Most critically, eq 1 was developed in the context of linear BCPs, such that its applicability to nonlinear architectures is uncertain.

Previous theoretical and simulation works have concluded that a cyclic BCP effectively behaves as a linear molecule of half the contour length.[9,23−25,27,40−42] However, this model apparently overestimates domain spacing reduction that should be achieved by cyclizing a linear diblock copolymer. For instance, on the basis of eq 1, Marko hypothesized that cyclic BCP domain size should scale as $(N/2)^{2/3}$ in the long chain limit,[23] implying that cyclization should reduce domain spacing by 37%. Meanwhile, the limited experimental data available comparing linear and cyclic diblock copolymers have found only 18−25% reductions.[30,31] In addition, experiment and simulation comparing the mean-square radius of gyration (R_g^2) of cyclic homopolymers in solution to that of their linear analogues have established that the *g*-factor ($g = R_{g,cyc}^2/R_{g,lin}^2$) for these molecules does not follow the $N/2$ prediction, instead ranging from 0.5 to 0.73 depending on molecular weight and solvent quality.[43−45]

Motivated by the challenge of meeting nanolithography design specifications for feature sizes, we use dissipative particle dynamic (DPD) simulation to quantify the dependence of BCP lamellar and HPC domain spacings on the experimentally tunable parameters χ, N, and polymer architecture (linear vs cyclic). We recognize that although it is well-established that nonconcatenation requirements force cyclic homopolymers in a melt to be significantly more compact than the Gaussian prediction,[46−52] the soft potentials used in DPD may allow nonphysical bond crossing to occur. However, the conformational impacts of nonconcatenation increase with chain length, and very short cyclic molecules show Gaussian scaling even in the melt state.[46,50,51,53−56] The high degree of coarse-graining in DPD makes DPD cyclic polymers necessarily very short, suggesting they are in a regime in which bond crossing will not impact the conformational statistics. Also, while there is a wealth of work quantifying the effects of nonconcatenation on cyclic homopolymer dimensions, its impacts on BCP domain spacing are unknown. It is not unreasonable to expect that nonconcatenation contributions to BCP free energy would be much smaller than the interblock repulsion and chain stretching forces, both of which are well-captured in the DPD representation.[25,39,57,58]

We therefore employ DPD in a first attempt to understand the interplay of chain length, chemistry, composition, and architecture in determining cyclic BCP domain spacings. Our simulations generate computational "experimental" results for linear and cyclic BCPs over a range of segregation strengths and degrees of polymerization. These data are analyzed within the context of SST with heuristic modifications that account for polymer architecture and localized chain stretching at the domain interface. Our revised scaling law is then applied to understand how cyclization of linear BCPs impacts self-assembly, illuminating the complex interplay of chain length, segregation strength, and architecture in determining BCP domain spacing and rationalizing the gap between theoretical predictions and experimental observations for feature size reduction by BCP cyclization.

2. MATERIALS AND METHODS

DPD is a coarse-grained simulation technique that represents the BCP as a chain of soft beads, each representing tens of monomers, connected by Hookean springs and interacting through soft pairwise forces. The high degree of coarse graining and softness of the interactions permits DPD to examine the phase behavior and microstructure of BCPs as a function of χ, N, f_A, and chain architecture.[25,39,57,59,60] A full description of the model can be found in the Supporting Information, but briefly, interparticle forces in DPD are broken up into a sum of pairwise conservative ($\mathbf{F}_{ij}^C$), dissipative ($\mathbf{F}_{ij}^D$), and random ($\mathbf{F}_{ij}^R$) forces between particles i and j. Interactions between bonded particles are modeled by using a Hookean spring ($\mathbf{F}_{ij}^S$), which enforces bead connectivity and polymer architecture. The conservative (energy-conserving) force enforces the chemical identity of the constituent coarse-grained bead, modeled in DPD as a soft repulsive interaction

$$\mathbf{F}_{ij}^C = \begin{cases} \dfrac{a_{ij}}{r_c}\left(1 - \dfrac{r_{ij}}{r_c}\right)\hat{\mathbf{r}}_{ij} & r_{ij} < r_c \\ 0 & r_{ij} \geq r_c \end{cases} \tag{2}$$

where a_{ij} is the DPD interaction parameter between beads i and j (dependent on the chemical identities of the interacting beads) that

DOI: 10.1021/acs.macromol.9b02015
Macromolecules 2019, 52, 9389−9397

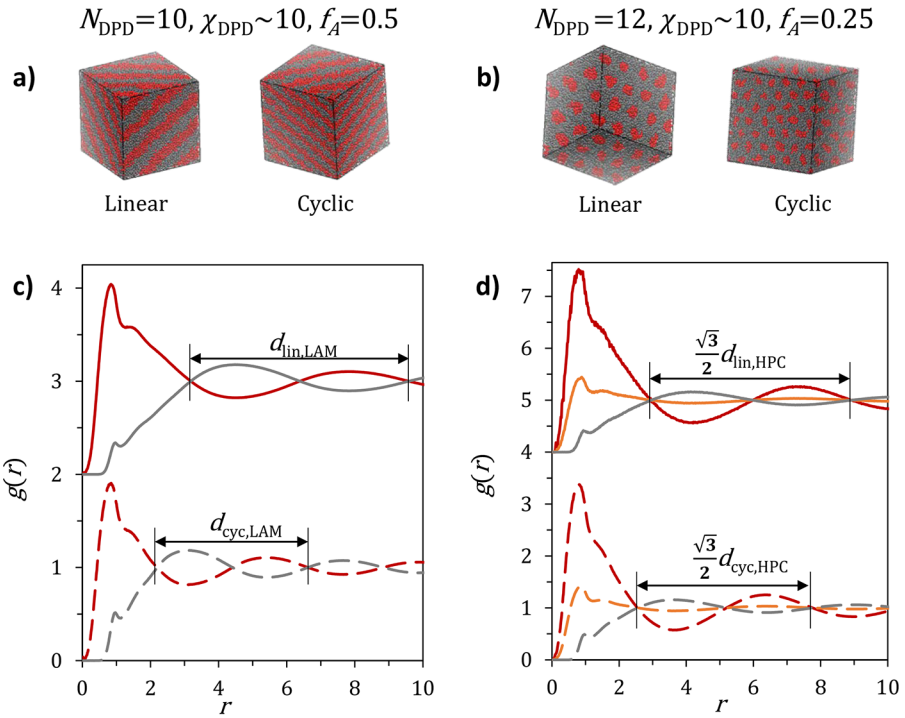

Figure 1. Effect of cyclization on nanoscale feature sizes formed by symmetric (f_A = 0.5) and asymmetric (f_A = 0.25) block copolymers. Images in (a) and (b) show VMD[72] renderings of the equilibrated structures, while the graphs in (c) and (d) demonstrate the use of radial distribution functions to measure domain spacing, *d*. *d* is related to the distance between the first and third (or *i* and *i* + 2) crossing points between $g_{AA}(r)$ (red trace), $g_{BB}(r)$ (orange), and $g_{AB}(r)$ (gray) as further described in the main text. Because of the symmetry of the lamellar phase, $g_{AA}(r) = g_{BB}(r)$ for the symmetric case shown in (c). Linear radial distribution functions in (c) and (d) have been shifted upward by an arbitrary amount for clarity.

represents the maximum repulsion at complete overlap, r_{ij} is the distance between interacting beads, $\hat{\mathbf{r}}_{ij} = \mathbf{r}_{ij}/r_{ij} = (\mathbf{r}_i - \mathbf{r}_j)/r_{ij}$ is the normalized direction vector pointing from *j* to *i*, and r_c is the cutoff distance after which interbead interactions vanish. For simplicity, we set r_c = 1 for all interbead interactions. The interaction between like beads, a_{AA} and a_{BB}, which is set to 25, establishes the compressibility of the system while the interaction between unlike beads, a_{AB}, controls miscibility between the two blocks. At a bead number density of ρ = 3 (the density of the simulations conducted here), the interbead interactions can be mapped to the Flory–Huggins χ parameter via the empirical correlation[57]

$$\chi = \frac{1}{3.27}(a_{AB} - a_{AA}) \tag{3}$$

We note that since DPD is a coarse-grained simulation technique, we cannot directly compare simulation and experimental values of χ. Rather, DPD values of χ are typically calculated to match the experimental segregation strengths, i.e., $\chi N_{BCP}|_{DPD} = \chi N_{BCP}|_{expt}$, to affect a meaningful comparison between simulation and experiment.[60] As discussed above, we recognize that the soft conservative force allows nonphysical bond crossing and ring concatenation to occur in DPD simulations. However, numerous simulations of BCPs with novel topologies such as cyclic, star, and π-shaped demonstrate that DPD captures the impacts of chain architecture on equilibrium polymer nanostructure including shifts in bulk morphology and feature size[61−63] and solution micelle formation.[64−67] In addition, Huang et al. demonstrated that adding a spring–spring repulsion to the DPD model (thus preventing bond crossing) had a negligible impact on the morphologies and characteristic sizes of nanostructures formed by BCPs of several different topologies.[61] Our simulation results show good agreement with experiment and strong segregation theory (see the Results and Discussion section), suggesting that bond crossing has a negligible effect on the minimum-energy conformations of the BCP systems studied here.

DPD simulations of linear (lin-A_mB_n) and cyclic (cyc-A_mB_n) BCP melts were performed using the LAMMPS software package.[68] The subscripts *m* and *n* indicate the number of monomers in the *A* and *B* blocks, respectively, so that the overall degree of polymerization is determined to be $N_{DPD} = m + n$. Both symmetric (f_A = 0.5), lamellae-forming and asymmetric (f_A = 0.25), hexagonally packed cylinder-forming systems were simulated. The Flory–Huggins parameter was varied from $3 < \chi_{DPD} < 40$, and the degree of polymerization ranged from $6 < N_{DPD} < 20$ for linear BCPs and $6 < N_{DPD} < 30$ for cyclic BCPs. The segregation strength was chosen to be sufficiently large ($\chi N > 30$) so that all the systems simulated here are expected to exhibit strong segregation-like domain scaling.[37,38] A plot of $d/(\chi_{DPD}{}^{1/6}N_{DPD}{}^{2/3})$ versus $(\chi N)_{DPD}$ supports the validity of this assumption (see the Supporting Information); the Supporting Information also includes a full list of the cyclic and linear BCP simulations performed in this work. All simulations consisted of 81000 total beads in a periodic, cubic simulation box with side length L = 30, corresponding to a bead number density of ρ = 3. Simulations were started from random initial configurations and equilibrated for at least 10^6 time steps. Following equilibration, production simulations were conducted for 5×10^5 time steps. Structural quantities were calculated from configurations generated during the production run by averaging over a minimum of 50 configurations evenly sampled over the entire production run.

3. RESULTS AND DISCUSSION

Above the ODT, symmetric linear and cyclic BCPs formed lamellae (LAM) and asymmetric (f_A = 0.25) polymers formed hexagonally packed cylinders (HPC) as shown in Figures 1a and 1b, consistent with experimental and theoretical phase diagrams. The characteristic dimension of the LAM (inter-lamellar spacing between *A* or *B* domains) and HPC (inter-rod center-to-center spacing) structures can be extracted from the radial distribution functions (RDFs) between polymer beads.

DOI: 10.1021/acs.macromol.9b02015
Macromolecules 2019, 52, 9389−9397

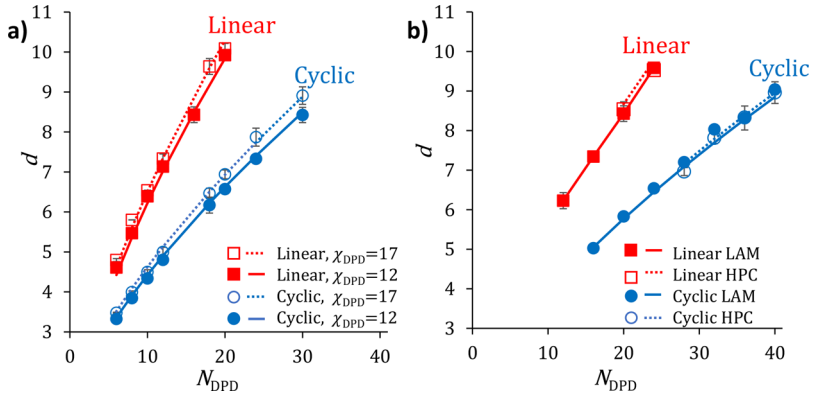

Figure 2. (a) Lamellar feature size scaling with N and χ. (b) Comparison of lamellar and HPC feature size scaling with N for χ_{DPD} = 4. In both figures, points represent domain spacings measured from DPD simulation, and lines are the fits to eq 4.

For the symmetric LAM morphology, the RDFs between like beads, $g_{AA}(r)$ and $g_{BB}(r)$, are equivalent and distinct from that between unlike beads, $g_{AB}(r)$. The interlamellar spacing is subsequently determined by the distance between the first and third crossing points between $g_{AA}(r)$ and $g_{AB}(r)$, which bound a single cycle of minima and maxima beyond the primary packing peak near $r \approx 1$,[69] as shown in Figure 1c.

In the cylindrical structure, the symmetry between $g_{AA}(r)$ and $g_{BB}(r)$ is broken due to the B monomers forming a continuous domain, while the A monomers are confined to a minority discontinuous domain. As a result, $g_{BB}(r)$ is relatively featureless compared to $g_{AA}(r)$, while $g_{AB}(r)$ for the HPC system is comparable to that for the LAM system (Figure 1d). The cylindrical domain spacing is defined as the distance between the first and third crossings of $g_{AA}(r)$ and $g_{AB}(r)$ multiplied by a factor of $\frac{2\sqrt{3}}{3}$ due to the hexagonal geometry of the system (see the Supporting Information).[70] Our RDF analysis consistently finds that cyclic BCPs form domains ≈30% smaller than their linear counterparts in both the LAM and HPC morphologies, demonstrating that DPD captures the impact of chain architecture on domain spacing. We note that BCP domain spacings can also be determined from static structure factors or from density profiles. In a previous work, we demonstrated that all three methods give results within 1% of each other.[71] We therefore only report spacings determined from the RDF method in this article.

Figure 2 illustrates the impacts of N, χ, and polymer architecture on feature sizes for the LAM (Figure 2a) and HPC (Figure 2b) morphologies. In agreement with eq 1, LAM domain spacings scale most strongly with N and comparatively weakly with χ. Additionally, linear domain spacings increase more sharply with N than those formed by cyclic polymers, regardless of morphology. Finally, the LAM and HPC domain sizes formed at a fixed χ display very similar scaling behavior with N, indicating the polymer molecular weight plays a dominant role in the domain size over the phase morphology. On the basis of these observations, we describe a heuristic modification of the SST scaling law (eq 1) that captures the impact of chain topology and finite chain length on LAM and HPC domain sizes.

Following the form established by SST, we propose that the BCP domain sizes are described as

$$d = \beta \chi^{\gamma} \Lambda^{\varepsilon} \tag{4}$$

where β and χ assume the same role as in eq 1, but N is replaced with the polymer "extent" embodied by the parameter Λ. Ideally the exponents γ and ε are 1/6 and 2/3, respectively; however, we treat them as adjustable parameters.

We model Λ as the product of two variables: λ, an architecture dependent term that grows with N, and σ, a correction that accounts for chain stretching at the interface (Figure 3). Considering random walk statistics[41,42,73] and

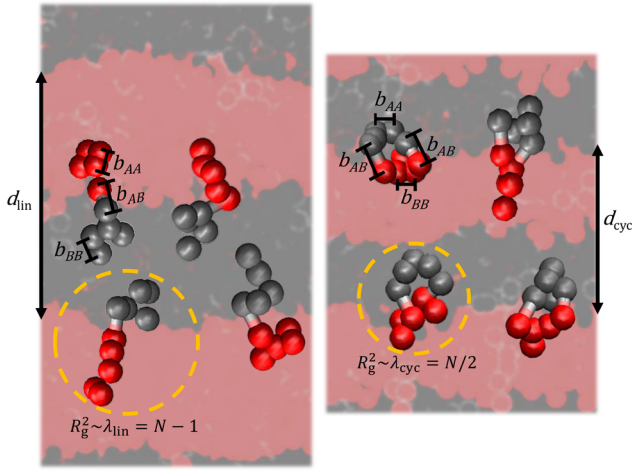

Figure 3. Snapshots from DPD simulations of the equilibrated systems of symmetric linear and cyclic BCPs ($N_{DPD} \sim 10$ and $\chi_{DPD} \sim 12$) with exemplary chain conformations demonstrating the components of eqs 4–7. λ is an architecture-dependent measure of overall polymer size, represented by the dashed yellow circle. Bonds between unlike monomers, b_{AB}, are ∼35% longer than those between like monomers, $b_{AA} = b_{BB}$; this interfacial stretching is incorporated into the revised scaling law through the term σ.

experimental observations[74] for polymer radius of gyration (R_g^2), we propose λ is determined to be the number of bonds in the polymer, which provides a measure of the contour length, divided by the number of bonds between unlike monomers. For the linear and cyclic polymers then

$$\lambda_{lin} = N - 1 \tag{5a}$$

and

$$\lambda_{cyc} = N/2 \tag{5b}$$

DOI: 10.1021/acs.macromol.9b02015
Macromolecules 2019, 52, 9389–9397

In the SST limit, $N \to \infty$ and $\lambda_{lin} \to N$ as expected. For the short, coarse-grained polymers simulated here, however, we must consider the finite polymer length.

A secondary concern to applying SST is that it assumes each polymer bond has the same average length. Even casual examination of the simulation snapshots in Figure 3, however, shows this assumption may not hold for the bonds pinned to the interface between the A and B domains. In fact, the bonds between unlike monomers seated at the domain interface, b_{AB}, are ~35% longer than those between like monomers, $b_{AA} = b_{BB}$. Because of the highly coarse-grained (i.e., very short) chains used in DPD simulation, the localized interfacial stretching contributes to the effective polymer length, especially for cyclic BCPs, which contain two $A-B$ bonds. Random walk theory finds that the impact of the localized stretching can be accounted for by the correction

$$\sigma = 1 + \frac{1}{\lambda}\left[\left(\frac{b_{AB}}{b_{AA}}\right)^2 - 1\right] \tag{6}$$

which corresponds to the ratio of the mean-square bond length of the actual BCP to the mean-square bond length assuming each bond is of length $b_{AA} = b_{BB}$ (see the Supporting Information).

The interfacial bond stretching in a DPD model mirrors differences observed experimentally between BCP chain conformations near the microphase interface compared to within the domain centers.[75,76] For example, Deloche and coworkers[76] used ^{2}H NMR to probe the orientations of PDMS chains in strongly segregated linear PS-*b*-PDMS copolymers and found that the PDMS chain segments near lamellar interfaces were oriented along the lamellar normal (and therefore made the strongest contributions to domain spacing); segment orientations gradually became more isotropic as distance from a PS block increased until chain segments in the center 14% (1.7 nm) of each PDMS block were randomly oriented. Therefore, while eq 6 may be unique to DPD simulation, the underlying physical concept of two $A-B$ bonds in a cyclic BCP magnifying the impacts of interfacial anisotropy on domain spacing is universal.

Combining eq 5 and eq 6 gives the polymer extent as

$$\Lambda = \lambda\sigma = \lambda + \left(\frac{b_{AB}}{b_{AA}}\right)^2 - 1 \tag{7}$$

Equation 7 reduces to the asymptotic linear ($\Lambda \sim N$) and cyclic ($\Lambda \sim N/2$) measures of polymer extent for infinitely long chains but accounts for the short chain length effects critical for translating scaling law predictions to experimental systems.

We performed a least-squares fit of the revised scaling law (eq 4) to our simulation results to determine β, γ, and ε. The ratio b_{AB}/b_{AA} was taken as 1.356 based on an average of bond length measurements from simulations of cyclic and linear BCPs (see the Supporting Information). As demonstrated by Matsen and Bates,[77] β depends on both f_A and BCP phase morphology. Therefore, we fit our results with two distinct prefactors, β_{LAM} and β_{HPC}. The fit parameters are reported in Table 1. The fitted exponents γ (= 0.140) and ε (= 0.653) closely match those predicted by SST (1/6 and 2/3), providing confidence in the physics underlying the model. The fitted prefactors β_{LAM} and β_{HPC} are nearly equal to one another, falling within theoretical predictions[78−81] that the two parameters differ by −4% to +6% for LAM ($f_A = 0.5$) and HPC ($f_A = 0.25$) phases. The lines in Figure 2 show the fit of eq 4 to the simulated domain spacings at selected χ values. We also compare our fit of eq 4 against all simulation results in Figure 4. Overall, the comparison is excellent with a root-mean-square error in the scaling model of 0.103, less than 2% of the measured domain spacings when all phase morphologies and chain architectures are considered.

Table 1. Fit Parameters of Eq 4 to the DPD Simulation Results[a]

β_{LAM}	0.832 ± 0.016
β_{HPC}	0.842 ± 0.018
γ	0.140 ± 0.005
ε	0.653 ± 0.007
b_{AB}/b_{AA}	1.356

[a]Error bars represent the 95% confidence interval determined by bootstrap resampling with 1000 iterations.

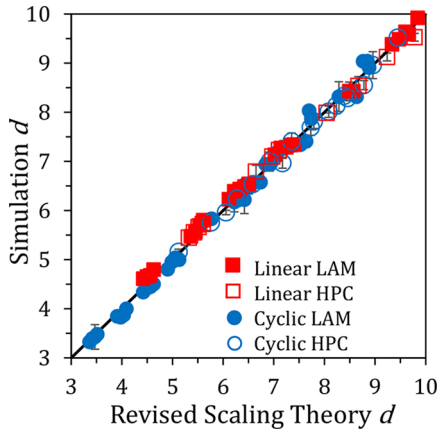

Figure 4. Parity plot comparing simulated domain spacings and model predictions. Overall, the RMS error between simulation and scaling theory eq 4 domain spacings is less than 2% of the measured d value.

To further validate our revised scaling law, we compare the predictions of eq 4 against the available experimental results. As noted above, a key motivation for utilizing cyclic polymers is to achieve smaller features using the same molecular weight polymer. Marko hypothesized that cyclic BCP domain size should scale as $(N/2)^{2/3}$ in the long chain limit,[23] which, when applied to eq 1, predicts cyclization reduces domain spacing by 37%, significantly more than the 18−25% reductions observed in experiment.[30,31] Our simulation results and eq 4, however, predict a significant chain length dependence of the fractional domain size reduction (Figure 5). As noted above, Poelma et al. found that cyclization of low molecular weight PS-*b*-PEO (M_n = 18 kg/mol, N_{exp} = 240) decreased the domain spacing by 25%. Our revised scaling law matches that prediction when $N_{DPD} = 6$, corresponding to a coarse-graining of 40 monomers per DPD bead. This degree of coarse-graining is well within the range where DPD accurately reproduces experiment.[25,39,57,58,82,83] Applying the same degree of coarse-graining to the Gartner et al. system of PS-*b*-POEGMA (M_n = 18 kg/mol, N_{exp} = 200) predicts a 21% decrease in domain spacing from cyclization, in agreement with the experimentally observed values (18−21%). The consistency of the χ and N scaling behavior for LAM and HPC features, recovery of the

DOI: 10.1021/acs.macromol.9b02015
Macromolecules 2019, 52, 9389−9397

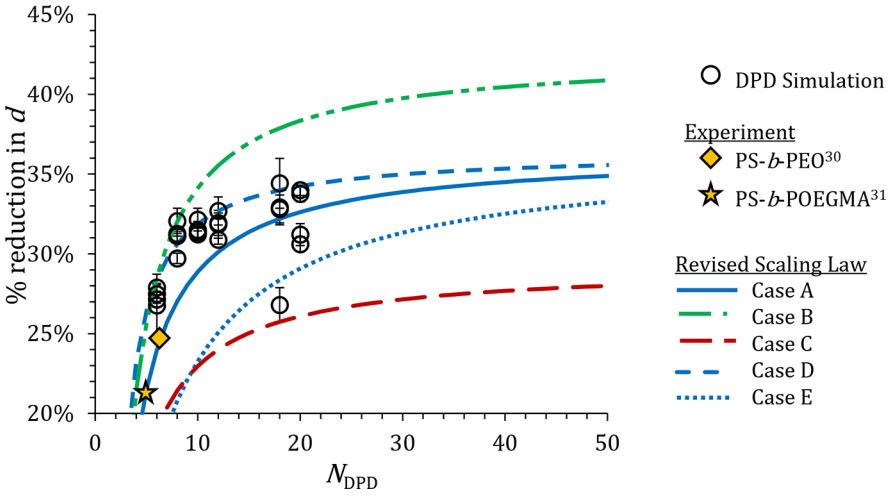

Figure 5. Percentage reduction in domain spacing, defined as $(d_{lin} - d_{cyc}) \times 100\%/d_{lin}$, obtained by cyclizing a linear diblock copolymer. Hollow circles represent domain spacing decreases measured from DPD simulation while the yellow symbols show the experimental results from ref 30 (diamond) and ref 31 (star). Lines give eq 4 predictions with different values of the scaling exponent ε and b_{AB}/b_{AA}. Case A: $\varepsilon = 0.653$, $b_{AB}/b_{AA} = 1.356$ (Table 1 values). Case B: $\varepsilon = 0.8$, $b_{AB}/b_{AA} = 1.356$. Case C: $\varepsilon = 0.5$, $b_{AB}/b_{AA} = 1.356$. Case D: $\varepsilon = 0.653$, $b_{AB}/b_{AA} = 1$. Case E: $\varepsilon = 0.653$, $b_{AB}/b_{AA} = 2$.

SST exponents and morphology-specific prefactors in eq 4, and match between eq 4 prediction and experimental results give us confidence in the revised scaling law to capture the impact of cyclic chain architecture on domain size. More critically, the revised scaling law shows that the ability of molecular cyclization to shrink BCP domain spacings decreases with polymer length, explaining why experimentalists have been unable to obtain the previously predicted ~40% reduction in feature size.

A key consequence of the revised scaling law is that the domain spacing of a cyclic BCP nanostructure can be predicted from that of its linear analogue. It is worthwhile, then, to consider the impact of scaling law parameter values on the decrease in feature size achievable through molecular cyclization. The β and χ contributions cancel when calculating the percent reduction (see the Supporting Information), indicating that domain shrinkage arises purely due to cyclization-induced changes in the polymer extent (Λ). The solid line in Figure 5 (case A) shows the reductions in domain spacing from molecular cyclization that would be predicted by eq 4 using the scaling exponents in Table 1. This prediction agrees with both our DPD simulations and reported experimental results. The lines in Figure 5 indicate that the finite chain length effects (see eqs 5a, 6, and 7) are significant up to $N_{DPD} \sim 20$. This DPD chain size corresponds to an experimental degree of polymerization of $N_{exp} = 800$, a chain length that would be challenging to synthesize and that would be unable to self-assemble into sub-10 nm features even in the cyclic architecture. We therefore conclude that the finite chain length effects are likely to be important in the vast majority of experimental cyclic BCPs. Note that the assignment $N \sim N_{exp}/40$ is specific to the DPD model employed here. To apply eq 4 to a more detailed model or experimental system, one would need to establish the appropriate definitions of N, which we anticipate would depend on physical properties of the specific polymer chains being studied, such as monomer volumes and persistence lengths. However, the impact of chain architecture on molecular size, as reflected by the definitions $\lambda_{lin} = N - 1$ and $\lambda_{cyc} = N/2$, should be model-independent.

Figure 5 also illustrates the impacts of non-SST scaling (ε) and interfacial elongation (b_{AB}/b_{AA}) on domain spacing. The maximum domain shrinkage occurs in the limit $N_{DPD} \to \infty$ at a plateau value of $(1 - 1/2^{\varepsilon}) \times 100\%$ (see the Supporting Information), suggesting ε has a strong impact on the ability of cyclization to reduce feature size. The $N^{0.653}$ scaling behavior found in this study means that cyclizing a very long, strongly segregated linear BCP will reduce d by 36%. However, in a regime where feature sizes scale more strongly with degree of polymerization such as the $d \sim N^{0.8}$ behavior of weakly segregated BCPs (i.e., $\chi N < 30$),[38,84] cyclic features may be more than 40% smaller than domains formed by their linear analogues (cases A, B, and C). In contrast, extended chain conformations at the interface counteract efforts to shrink feature sizes (cases A, D, and E). Because a cyclic polymer has twice as many interfacial bonds as a linear BCP, the ability of cyclization to shrink BCP feature sizes decreases as b_{AB}/b_{AA} increases and as N decreases. In summary, decreasing N will directly reduce d by decreasing λ and promote further reduction in d upon cyclization if the polymer enters the weak segregation regime, but interfacial stretching of polymer chains (higher b_{AB}/b_{AA}) will limit the percent reduction in d achievable by cyclization. Thus, experimentalists seeking to reduce domain sizes by cyclization must consider finite chain length effects, the scaling regime in which they are operating, and how the specific block chemistries may affect interfacial conformations.

4. CONCLUSIONS

We have systematically explored the relationship between the degree of polymerization, chemistry, and block volume fraction in determining domain sizes of self-assembled linear and cyclic BCPs. Previous experimental studies conducted with relatively short polymers found cyclization decreases BCP domain spacing by 18−25%, whereas prior theoretical work predicted domain shrinkage up to 40% in the long-chain limit. Our revised scaling law provides important insights into physics underlying cyclic BCP self-assembly that account for the discrepancy between experiment and theory. First, it establishes that the size of a BCP chain depends on the

DOI: 10.1021/acs.macromol.9b02015
Macromolecules 2019, 52, 9389−9397

number of bonds in the molecule and the number of times the chain crosses the interface in its self-assembled state. Second, it highlights how increased BCP anisotropy around interfacial bonds (captured by the σ term) impacts equilibrium feature size and the role this phenomenon plays in swelling cyclic BCP domain spacings beyond what strong segregation theory would predict. While the exact equations presented herein have been developed from coarse-grained simulation results, these underlying physics should be universal. Overall then, the revised scaling law provides a method for predicting BCP feature sizes based on experimentally tunable parameters and also highlights key challenges in developing polymers for next generation BCP lithography by manipulating chain architectures.

■ ASSOCIATED CONTENT

Supporting Information

The Supporting Information is available free of charge at https://pubs.acs.org/doi/10.1021/acs.macromol.9b02015.

DPD simulation methods; HPC domain spacing calculation from radial distribution functions; domain spacing measurements from simulation; derivation of σ from random walk statistics; predicting percent reduction in lamellar size from cyclization (PDF)

■ AUTHOR INFORMATION

Corresponding Authors

*E-mail hanka@tulane.edu.
*E-mail jalbert6@tulane.edu.

ORCID

Amy D. Goodson: 0000-0002-5596-9033
Henry S. Ashbaugh: 0000-0001-9869-1900
Julie N. L. Albert: 0000-0002-6000-9408

Notes

The authors declare no competing financial interest.

■ ACKNOWLEDGMENTS

The authors gratefully acknowledge support from the National Science Foundation through a Graduate Research Fellowship (A.D.G., Grant B55600G1), NSF-CMMI Grant 1825881, and NSF-DMR-REU Grants 1460637 and 1852275. Additional support for this work came from the Robert and Gayle Longmire Early Career Professorship in Chemical Engineering (J.N.L.A.).

■ REFERENCES

(1) Dammel, R. R. Cost-effective sub-20 nm lithography: smart chemicals to the rescue. *J. Photopolym. Sci. Technol.* **2011**, *24* (1), 33−42.
(2) Beyond the diffraction limit. *Nat. Photonics* **2009**, *3*, 361.
(3) Bates, F. S. Polymer-polymer phase behavior. *Science* **1991**, *251* (4996), 898−905.
(4) Bates, F. S.; Fredrickson, G. H. Block Copolymer Thermodynamics: Theory and Experiment. *Annu. Rev. Phys. Chem.* **1990**, *41* (1), 525−557.
(5) Lo, T.-Y.; Krishnan, M. R.; Lu, K.-Y.; Ho, R.-M. Silicon-containing block copolymers for lithographic applications. *Prog. Polym. Sci.* **2018**, *77*, 19−68.
(6) Farnham, W.; Sheehan, M. RAFT synthesis of block copolymers and their self-assembly properties. In *Directed Self-assembly of Block Co-polymers for Nano-manufacturing*; Elsevier: 2015; pp 27−45.
(7) Maher, M. J.; Rettner, C. T.; Bates, C. M.; Blachut, G.; Carlson, M. C.; Durand, W. J.; Ellison, C. J.; Sanders, D. P.; Cheng, J. Y.; Willson, C. G. Directed self-assembly of silicon-containing block copolymer thin films. *ACS Appl. Mater. Interfaces* **2015**, *7* (5), 3323−3328.
(8) Kim, J. M.; Hur, Y. H.; Jeong, J. W.; Nam, T. W.; Lee, J. H.; Jeon, K.; Kim, Y.; Jung, Y. S. Block Copolymer with an Extremely High Block-to-Block Interaction for a Significant Reduction of Line-Edge Fluctuations in Self-Assembled Patterns. *Chem. Mater.* **2016**, *28* (16), 5680−5688.
(9) Lescanec, R. L.; Hajduk, D. A.; Kim, G. Y.; Gan, Y.; Yin, R.; Gruner, S. M.; Hogen-Esch, T. E.; Thomas, E. L. Comparison of the Lamellar Morphology of Microphase-Separated Cyclic Block Copolymers and Their Linear Precursors. *Macromolecules* **1995**, *28* (9), 3485−3489.
(10) Takano, A.; Nonaka, A.; Kadoi, O.; Hirahara, K.; Kawahara, S.; Isono, Y.; Torikai, N.; Matsushita, Y. Preparation and characterization of cyclic polystyrene with short poly (2-tert-butylbutadiene) sequences. *J. Polym. Sci., Part B: Polym. Phys.* **2002**, *40* (15), 1582−1589.
(11) Zhu, Y.; Gido, S. P.; Iatrou, H.; Hadjichristidis, N.; Mays, J. W. Microphase separation of cyclic block copolymers of styrene and butadiene and of their corresponding linear triblock copolymers. *Macromolecules* **2003**, *36* (1), 148−152.
(12) Isono, T.; Otsuka, I.; Kondo, Y.; Halila, S.; Fort, S.; Rochas, C.; Satoh, T.; Borsali, R.; Kakuchi, T. Sub-10 nm Nano-Organization in AB2- and AB3-Type Miktoarm Star Copolymers Consisting of Maltoheptaose and Polycaprolactone. *Macromolecules* **2013**, *46* (4), 1461−1469.
(13) Isono, T.; Kawakami, N.; Watanabe, K.; Yoshida, K.; Otsuka, I.; Mamiya, H.; Ito, H.; Yamamoto, T.; Tajima, K.; Borsali, R.; Satoh, T. Microphase Separation of Carbohydrate-Based Star-Block Copolymers with Sub-10 nm Periodicity. *Polym. Chem.* **2019**, *10* (9), 1119−1129.
(14) Shi, W.; Tateishi, Y.; Li, W.; Hawker, C. J.; Fredrickson, G. H.; Kramer, E. J. Producing Small Domain Features Using Miktoarm Block Copolymers with Large Interaction Parameters. *ACS Macro Lett.* **2015**, *4* (11), 1287−1292.
(15) Minehara, H.; Pitet, L. M.; Kim, S.; Zha, R. H.; Meijer, E. W.; Hawker, C. J. Branched Block Copolymers for Tuning of Morphology and Feature Size in Thin Film Nanolithography. *Macromolecules* **2016**, *49* (6), 2318−2326.
(16) Sun, Z.; Zhang, W.; Hong, S.; Chen, Z.; Liu, X.; Xiao, S.; Coughlin, E. B.; Russell, T. P. Using block copolymer architecture to achieve sub-10 nm periods. *Polymer* **2017**, *121*, 297−303.
(17) Mayes, A. M.; Olvera de la Cruz, M. Microphase separation in multiblock copolymer melts. *J. Chem. Phys.* **1989**, *91* (11), 7228−7235.
(18) Matsen, M. W.; Thompson, R. Equilibrium behavior of symmetric ABA triblock copolymer melts. *J. Chem. Phys.* **1999**, *111* (15), 7139−7146.
(19) Kelly, G. M.; Haque, F. M.; Grayson, S. M.; Albert, J. N. L. Suppression of Melt-Induced Dewetting in Cyclic Poly (ϵ-caprolactone) Thin Films. *Macromolecules* **2017**, *50* (24), 9852−9856.
(20) McLeish, T. Polymers without beginning or end. *Science* **2002**, *297* (5589), 2005−2006.
(21) Habuchi, S.; Satoh, N.; Yamamoto, T.; Tezuka, Y.; Vacha, M. Multimode diffusion of ring polymer molecules revealed by a single-molecule study. *Angew. Chem., Int. Ed.* **2010**, *49* (8), 1418−1421.
(22) Habuchi, S.; Fujiwara, S.; Yamamoto, T.; Vacha, M.; Tezuka, Y. Single-molecule study on polymer diffusion in a melt state: Effect of chain topology. *Anal. Chem.* **2013**, *85* (15), 7369−7376.
(23) Marko, J. Microphase separation of block copolymer rings. *Macromolecules* **1993**, *26* (6), 1442−1444.
(24) Zhang, G.; Fan, Z.; Yang, Y.; Qiu, F. Phase behaviors of cyclic diblock copolymers. *J. Chem. Phys.* **2011**, *135* (17), 174902.
(25) Qian, H.-J.; Lu, Z.-Y.; Chen, L.-J.; Li, Z.-S.; Sun, C.-C. Computer Simulation of Cyclic Block Copolymer Microphase Separation. *Macromolecules* **2005**, *38* (4), 1395−1401.

DOI: 10.1021/acs.macromol.9b02015
Macromolecules 2019, 52, 9389−9397

(26) Jo, W. H.; Jang, S. S. Monte Carlo simulation of the order-disorder transition of a symmetric cyclic diblock copolymer system. *J. Chem. Phys.* **1999**, *111* (4), 1712−1720.
(27) Weyersberg, A.; Vilgis, T. A. Microphase separation in topologically constrained ring copolymers. *Phys. Rev. E: Stat. Phys., Plasmas, Fluids, Relat. Interdiscip. Top.* **1994**, *49* (4), 3097−3101.
(28) Takano, A.; Kadoi, O.; Hirahara, K.; Kawahara, S.; Isono, Y.; Suzuki, J.; Matsushita, Y. Preparation and Morphology of Ring-Shaped Polystyrene-*block*-polyisoprenes. *Macromolecules* **2003**, *36* (9), 3045−3050.
(29) Ryan, A. J.; Mai, S.-M.; Fairclough, J. P. A.; Hamley, I. W.; Booth, C. Ordered melts of block copolymers of ethylene oxide and 1, 2-butylene oxide. *Phys. Chem. Chem. Phys.* **2001**, *3* (15), 2961−2971.
(30) Poelma, J. E.; Ono, K.; Miyajima, D.; Aida, T.; Satoh, K.; Hawker, C. J. Cyclic Block Copolymers for Controlling Feature Sizes in Block Copolymer Lithography. *ACS Nano* **2012**, *6* (12), 10845−10854.
(31) Gartner, T. E.; Kubo, T.; Seo, Y.; Tansky, M.; Hall, L. M.; Sumerlin, B. S.; Epps, T. H. Domain Spacing and Composition Profile Behavior in Salt-Doped Cyclic vs Linear Block Polymer Thin Films: A Joint Experimental and Simulation Study. *Macromolecules* **2017**, *50* (18), 7169−7176.
(32) Likhtman, A.; Semenov, A. An advance in the theory of strongly segregated polymers. *EPL (Europhysics Letters)* **2000**, *51* (3), 307−313.
(33) Semenov, A. Contribution to the theory of microphase layering in block-copolymer melts. *Zh. Eksp. Teor. Fiz.* **1985**, *88* (4), 1242−1256.
(34) Semenov, A. Theory of block copolymer interfaces in the strong segregation limit. *Macromolecules* **1993**, *26* (24), 6617−6621.
(35) Matsen, M. W. The standard Gaussian model for block copolymer melts. *J. Phys.: Condens. Matter* **2002**, *14* (2), R21−R47.
(36) Hadjichristidis, N.; Pispas, S.; Floudas, G. *Block Copolymers: Synthetic Strategies, Physical Properties, and Applications*; John Wiley & Sons: 2003.
(37) Matsushita, Y.; Mori, K.; Saguchi, R.; Nakao, Y.; Noda, I.; Nagasawa, M. Molecular weight dependence of lamellar domain spacing of diblock copolymers in bulk. *Macromolecules* **1990**, *23* (19), 4313−4316.
(38) Papadakis, C. M.; Almdal, K.; Mortensen, K.; Posselt, D. A small-angle scattering study of the bulk structure of a symmetric diblock copolymer system. *J. Phys. II* **1997**, *7* (12), 1829−1854.
(39) Gavrilov, A. A.; Kudryavtsev, Y. V.; Chertovich, A. V. Phase diagrams of block copolymer melts by dissipative particle dynamics simulations. *J. Chem. Phys.* **2013**, *139* (22), 224901.
(40) Ryan, A. J.; Mai, S.-M.; Fairclough, J. P. A.; Hamley, I. W.; Booth, C. Ordered melts of block copolymers of ethylene oxide and 1,2-butylene oxide. *Phys. Chem. Chem. Phys.* **2001**, *3* (15), 2961−2971.
(41) Kramers, H. A. The behavior of macromolecules in inhomogeneous flow. *J. Chem. Phys.* **1946**, *14* (7), 415−424.
(42) Zimm, B. H.; Stockmayer, W. H. The Dimensions of Chain Molecules Containing Branches and Rings. *J. Chem. Phys.* **1949**, *17* (12), 1301−1314.
(43) Gartner III, T. E.; Haque, F. M.; Gomi, A. M.; Grayson, S. M.; Hore, M. J.; Jayaraman, A. Scaling Exponent and Effective Interactions in Linear and Cyclic Polymer Solutions: Theory, Simulations, and Experiments. *Macromolecules* **2019**, *52* (12), 4579−4589.
(44) Takano, A.; Ohta, Y.; Masuoka, K.; Matsubara, K.; Nakano, T.; Hieno, A.; Itakura, M.; Takahashi, K.; Kinugasa, S.; Kawaguchi, D.; Takahashi, Y.; Matsushita, Y. Radii of Gyration of Ring-Shaped Polystyrenes with High Purity in Dilute Solutions. *Macromolecules* **2012**, *45* (1), 369−373.
(45) Halverson, J. D.; Lee, W. B.; Grest, G. S.; Grosberg, A. Y.; Kremer, K. Molecular dynamics simulation study of nonconcatenated ring polymers in a melt. I. Statics. *J. Chem. Phys.* **2011**, *134* (20), 204904.
(46) Cates, M.; Deutsch, J. Conjectures on the statistics of ring polymers. *J. Phys. (Paris)* **1986**, *47* (12), 2121−2128.
(47) Hur, K.; Winkler, R. G.; Yoon, D. Y. Comparison of ring and linear polyethylene from molecular dynamics simulations. *Macromolecules* **2006**, *39* (12), 3975−3977.
(48) Iyer, B. V.; Lele, A. K.; Shanbhag, S. What Is the Size of a Ring Polymer in a Ring- Linear Blend? *Macromolecules* **2007**, *40* (16), 5995−6000.
(49) Jeong, C.; Douglas, J. F. Relation between polymer conformational structure and dynamics in linear and ring polyethylene blends. *Macromol. Theory Simul.* **2017**, *26* (5), 1700045.
(50) Müller, M.; Wittmer, J.; Cates, M. Topological effects in ring polymers: A computer simulation study. *Phys. Rev. E: Stat. Phys., Plasmas, Fluids, Relat. Interdiscip. Top.* **1996**, *53* (5), 5063−5074.
(51) Richter, D.; Gooßen, S.; Wischnewski, A. Celebrating Soft Matter's 10th Anniversary: Topology matters: structure and dynamics of ring polymers. *Soft Matter* **2015**, *11* (44), 8535−8549.
(52) Arrighi, V.; Gagliardi, S.; Dagger, A.; Semlyen, J.; Higgins, J.; Shenton, M. Conformation of cyclics and linear chain polymers in bulk by SANS. *Macromolecules* **2004**, *37* (21), 8057−8065.
(53) Halverson, J. D.; Grest, G. S.; Grosberg, A. Y.; Kremer, K. Rheology of ring polymer melts: From linear contaminants to ring-linear blends. *Phys. Rev. Lett.* **2012**, *108* (3), 038301.
(54) Pakula, T.; Geyler, S. Cooperative relaxations in condensed macromolecular systems. 3. Computer-simulated melts of cyclic polymers. *Macromolecules* **1988**, *21* (6), 1665−1670.
(55) Vettorel, T.; Grosberg, A. Y.; Kremer, K. Statistics of polymer rings in the melt: a numerical simulation study. *Phys. Biol.* **2009**, *6* (2), 025013.
(56) Brown, S.; Lenczycki, T.; Szamel, G. Influence of topological constraints on the statics and dynamics of ring polymers. *Phys. Rev. E: Stat. Phys., Plasmas, Fluids, Relat. Interdiscip. Top.* **2001**, *63* (5), 052801.
(57) Groot, R. D.; Madden, T. J. Dynamic simulation of diblock copolymer microphase separation. *J. Chem. Phys.* **1998**, *108* (20), 8713−8724.
(58) Groot, R. D.; Madden, T. J.; Tildesley, D. J. On the role of hydrodynamic interactions in block copolymer microphase separation. *J. Chem. Phys.* **1999**, *110* (19), 9739−9749.
(59) Posel, Z.; Lísal, M.; Brennan, J. K. Interplay between microscopic and macroscopic phase separations in ternary polymer melts: Insight from mesoscale modelling. *Fluid Phase Equilib.* **2009**, *283* (1), 38−48.
(60) Soto-Figueroa, C.; Rodríguez-Hidalgo, M.-d.-R.; Martínez-Magadán, J.-M.; Vicente, L. Dissipative Particle Dynamics Study of Order-Order Phase Transition of BCC, HPC, OBDD, and LAM Structures of the Poly(styrene)-Poly(isoprene) Diblock Copolymer. *Macromolecules* **2008**, *41* (9), 3297−3304.
(61) Huang, C. I.; Yang, L. F.; Lin, C. H.; Yu, H. T. A Comparison of Y-, H-, and π-shaped Diblock Copolymers via Dissipative Particle Dynamics. *Macromol. Theory Simul.* **2008**, *17* (4−5), 198−207.
(62) Xu, Y.; Feng, J.; Liu, H.; Hu, Y. Microphase separation of star-diblock copolymer melts studied by dissipative particle dynamics simulation. *Mol. Simul.* **2006**, *32* (5), 375−383.
(63) Soto-Figueroa, C.; Vicente, L.; Martínez-Magadán, J.-M.; Rodríguez-Hidalgo, M.-d.-R. Self-Organization Process of Ordered Structures in Linear and Star Poly (styrene)- Poly (isoprene) Block Copolymers: Gaussian Models and Mesoscopic Parameters of Polymeric Systems. *J. Phys. Chem. B* **2007**, *111* (40), 11756−11764.
(64) Lin, C.-M.; Chen, Y.-Z.; Sheng, Y.-J.; Tsao, H.-K. Effects of macromolecular architecture on the micellization behavior of complex block copolymers. *React. Funct. Polym.* **2009**, *69* (7), 539−545.
(65) Wang, J.; Li, J.; Yao, Q.; Sun, X.; Yan, Y.; Zhang, J. One-pot production of porous assemblies by PISA of star architecture copolymers: a simulation study. *Phys. Chem. Chem. Phys.* **2018**, *20* (15), 10069−10076.
(66) Zhao, Y.; Liu, Y.-T.; Lu, Z.-Y.; Sun, C.-C. Effect of molecular architecture on the morphology diversity of the multicompartment

DOI: 10.1021/acs.macromol.9b02015
Macromolecules 2019, 52, 9389−9397

micelles: A dissipative particle dynamics simulation study. *Polymer* **2008**, *49* (22), 4899−4909.
(67) Xia, J.; Liu, D.; Zhong, C. Multicompartment micelles and vesicles from π-shaped ABC block copolymers: A dissipative particle dynamics study. *Phys. Chem. Chem. Phys.* **2007**, *9* (38), 5267−5273.
(68) Plimpton, S. Fast Parallel Algorithms for Short-Range Molecular Dynamics. *J. Comput. Phys.* **1995**, *117* (1), 1−19.
(69) Li, Y.; Qian, H.-J.; Lu, Z.-Y. The influence of one block polydispersity on phase separation of diblock copolymers: The molecular mechanism for domain spacing expansion. *Polymer* **2013**, *54* (14), 3716−3722.
(70) Tanaka, H.; Hasegawa, H.; Hashimoto, T. Ordered structure in mixtures of a block copolymer and homopolymers. 1. Solubilization of low molecular weight homopolymers. *Macromolecules* **1991**, *24* (1), 240−251.
(71) Goodson, A. D.; Liu, G.; Rick, M. S.; Raymond, A. W.; Uddin, M. F.; Ashbaugh, H. S.; Albert, J. N. L. Nanostructure stability and swelling of ternary block copolymer/homopolymer blends: A direct comparison between dissipative particle dynamics and experiment. *J. Polym. Sci., Part B: Polym. Phys.* **2019**, *57* (12), 794−803.
(72) Humphrey, W.; Dalke, A.; Schulten, K. VMD: Visual molecular dynamics. *J. Mol. Graphics* **1996**, *14* (1), 33−38.
(73) Rubinstein, M.; Colby, R. H. *Polymer Physics*; Oxford University Press: New York, 2003; Vol. *23*.
(74) Hadziioannou, G.; Cotts, P. M.; Ten Brinke, G.; Han, C. C.; Lutz, P.; Strazielle, C.; Rempp, P.; Kovacs, A. J. Thermodynamic and hydrodynamic properties of dilute solutions of cyclic and linear polystyrenes. *Macromolecules* **1987**, *20* (3), 493−497.
(75) Matsushita, Y.; Mori, K.; Mogi, Y.; Saguchi, R.; Noda, I.; Nagasawa, M.; Chang, T.; Glinka, C. J.; Han, C. C. Chain conformation of a block polymer in a microphase-separated structure. *Macromolecules* **1990**, *23* (19), 4317−4321.
(76) Lorthioir, C.; Randriamahefa, S.; Deloche, B. Some aspects of the orientational order distribution of flexible chains in a diblock mesophase. *J. Chem. Phys.* **2013**, *139* (22), 224903.
(77) Matsen, M.; Bates, F. Block copolymer microstructures in the intermediate-segregation regime. *J. Chem. Phys.* **1997**, *106* (6), 2436−2448.
(78) Helfand, E. Block copolymer theory. III. Statistical mechanics of the microdomain structure. *Macromolecules* **1975**, *8* (4), 552−556.
(79) Helfand, E.; Wasserman, Z. Block copolymer theory. 5. Spherical domains. *Macromolecules* **1978**, *11* (5), 960−966.
(80) Helfand, E.; Wasserman, Z. Block copolymer theory. 6. Cylindrical domains. *Macromolecules* **1980**, *13* (4), 994−998.
(81) Likhtman, A. E.; Semenov, A. N. Stability of the OBDD structure for diblock copolymer melts in the strong segregation limit. *Macromolecules* **1994**, *27* (11), 3103−3106.
(82) Vázquez-Quesada, A.; Ellero, M.; Español, P. Consistent scaling of thermal fluctuations in smoothed dissipative particle dynamics. *J. Chem. Phys.* **2009**, *130* (3), 034901.
(83) Martínez-Veracoechea, F. J.; Escobedo, F. A. Simulation of the gyroid phase in off-lattice models of pure diblock copolymer melts. *J. Chem. Phys.* **2006**, *125* (10), 104907.
(84) Almdal, K.; Rosedale, J. H.; Bates, F. S.; Wignall, G. D.; Fredrickson, G. H. Gaussian- to stretched-coil transition in block copolymer melts. *Phys. Rev. Lett.* **1990**, *65* (9), 1112−1115.

DOI: 10.1021/acs.macromol.9b02015
Macromolecules 2019, 52, 9389−9397

Supporting Information for

Impact of cyclic block copolymer chain architecture and degree of polymerization on nanoscale domain spacing: a simulation and scaling theory analysis

Amy D. Goodson,[1] Jessie E. Troxler,[1] Maxwell S. Rick[1], Henry S. Ashbaugh,[1*] and Julie N. L. Albert[1*]

[1]Department of Chemical and Biomolecular Engineering, Tulane University, New Orleans, Louisiana 70118, United States of America

[*]Address correspondence to hanka@tulane.edu and jalbert6@tulane.edu.

Section 1: DPD Simulation Methods

Dissipative particle dynamics (DPD) is a coarse-grained simulation technique that represents the block copolymer (BCP) as a chain of soft beads, each representing 10s of monomers, connected by Hookean springs. The high degree of coarse graining and softness of the interactions permits DPD to examine the phase behavior and meso-scale structure of BCPs and polymer blends as a function of χ, N, f_A, and chain architecture.[1-5] Significantly, DPD retains the inherent thermal fluctuations eliminated from mean field theories that can be significant in polymer phase behavior.[1, 6-8]

Interparticle forces in DPD are broken up into a sum of pairwise conservative ($\boldsymbol{F}_{ij}^{C}$), dissipative ($\boldsymbol{F}_{ij}^{D}$), and random ($\boldsymbol{F}_{ij}^{R}$) forces between particles i and j. Interactions between bonded particles are modeled using a Hookean spring ($\boldsymbol{F}_{ij}^{S}$), which enforces bead connectivity and polymer architecture. The net force on DPD bead *i* is subsequently determined as a sum over interactions with all other beads in the simulation[14,15]

$$\boldsymbol{F}_i = \sum_{j \neq i} \boldsymbol{F}_{ij}^{C} + \boldsymbol{F}_{ij}^{D} + \boldsymbol{F}_{ij}^{R} + \boldsymbol{F}_{ij}^{S}. \tag{S1}$$

This force governs the time evolution of the particle system according to Newton's Laws of Motion; our simulations use the velocity Verlet algorithm[9] with a timestep $\Delta t = 0.025$. The mass of each bead in the simulation is assumed to be m = 1.

The conservative (energy-conserving) force enforces the chemical identity of the constituent coarse-grained bead, modeled in DPD as a soft repulsive interaction

$$\boldsymbol{F}_{ij}^{C} = \begin{cases} \frac{a_{ij}}{r_c}\left(1 - \frac{r_{ij}}{r_c}\right)\hat{\boldsymbol{r}}_{ij} & r_{ij} < r_c \\ 0 & r_{ij} \geq r_c \end{cases}, \tag{S2}$$

where a_{ij} is the DPD interaction parameter between beads i and j (dependent on the chemical identities of the interacting beads) that represents the maximum repulsion at complete overlap; r_{ij}

is the distance between interacting beads; $\hat{\boldsymbol{r}}_{ij} = \boldsymbol{r}_{ij}/r_{ij} = (\boldsymbol{r}_i - \boldsymbol{r}_j)/r_{ij}$ is the normalized direction vector pointing from j to i; and r_c is the cut-off distance after which inter-bead interactions vanish. For simplicity, we set r_c = 1 for all inter-bead interactions. The interaction between like beads, a_{AA} and $a_{\mathrm{BB,}}$ which is set to 25, establishes the compressibility of the system while the interaction between unlike beads, a_{AB}, controls miscibility between the two blocks.[14] At a bead number density of ρ = 3 (the density of the simulations conducted here), the inter-bead interactions can be mapped to the Flory-Huggins χ parameter via the empirical correlation[1]

$$\chi = \frac{1}{3.27}(a_{\mathrm{AB}} - a_{\mathrm{AA}}). \tag{S3}$$

We note that since DPD is a coarse-grained simulation technique, we cannot directly compare simulation and experimental values of χ. Rather, DPD values of χ are typically calculated to match the experimental segregation strengths, i.e., $\chi N_{\mathrm{BCP}}|_{\mathrm{DPD}} = \chi N_{\mathrm{BCP}}|_{\mathrm{expt}}$, to affect a meaningful comparison between simulation and experiment.[5]

The dissipative force accounts for the viscous drag of the multiple atomic sites condensed onto a single coarse-grained bead. DPD models the dissipative force as

$$\boldsymbol{F}_{ij}^{D} = -\gamma\omega_{ij}^{D}(r_{ij})(\boldsymbol{v}_{ij}\cdot\boldsymbol{r}_{ij})\hat{\boldsymbol{r}}_{ij}, \tag{S4}$$

where γ is the friction coefficient, and $\boldsymbol{v}_{ij} = \boldsymbol{v}_i - \boldsymbol{v}_j$ is the relative velocity between particles i and j. The random force accounts for thermal Brownian kicks from the coarsened degrees of freedom, modeled in DPD as

$$\boldsymbol{F}_{ij}^{R} = -\sigma\omega_{ij}^{R}(r_{ij})\frac{\zeta_{ij}}{\sqrt{\Delta t}}\hat{\boldsymbol{r}}_{ij}, \tag{S5}$$

where σ is a constant noise amplitude related to the temperature, and ζ_{ij} is a Gaussian random number with a mean of zero and unit variance. The fluctuation dissipation theorem imposes the

following constraints on the distance dependent weight functions $\omega_{ij}^{D}(r)$ and $\omega_{ij}^{R}(r)$ and the amplitudes of the viscous and random forces[10]:

$$\omega_{ij}^{D}(r_{ij}) = \left[\omega_{ij}^{R}(r_{ij})\right]^2 \tag{S6a}$$

and

$$\sigma^2 = 2\gamma k_B T, \tag{S6b}$$

where $k_B T$ is the product of the Boltzmann's constant and the absolute temperature. Taken together then, eqs. (S4-S6) act as a thermostat ensuring DPD simulations sample the canonical (constant NVT) ensemble. Since the form of one of the weighting functions appearing in eq. (S4 and eq. (S5) is arbitrary, for simplicity DPD simulations adopt the expression

$$\omega_{ij}^{D}(r_{ij}) = \left[\omega_{ij}^{R}(r_{ij})\right]^2 = \begin{cases} \left(1 - \frac{r_{ij}}{r_c}\right)^2 & r_{ij} < r_c, \\ 0 & r_{ij} \geq r_c \end{cases} \tag{S7}$$

which vanishes beyond r_c, like the conservative force. Here, we assume $k_B T$ = 1 and σ = 3 (γ = 4.5) as recommended in ref. 6 to ensure fast, stable simulations.

Finally, the Hookean spring force in eq. (S1) is a second conservative interaction only between bonded beads that enforces intramolecular polymer connectivity. The spring force is evaluated as

$$F_{ij}^{S} = k r_{ij} \hat{\mathbf{r}}_{ij}, \tag{S8}$$

where k is the spring constant, assumed here to be equal to 4,[1, 7] independent of the chemical identity of the bonded monomers.

Section 2: HPC Domain Spacing Calculation from Radial Distribution Functions

While others have demonstrated the use of RDFs to measure lamellar domain sizes,[11] we are unaware of references using RDFs to measure HPC structures. To confirm the approach's validity, we calculated the "ideal" RDFs for an HPC structure formed by a BCP with $f_A = 0.25$ and compared these to the known domain spacing. We randomly selected 10^6 points in an $8 \times 4\sqrt{3} \times 10$ box and identified the points as being located within a minority (cylindrical) or majority (matrix) domain based on the Figure S1 inset geometry. We then generated $g_{AA}(r)$, $g_{BB}(r)$, and $g_{AB}(r)$ between all of these points as shown in Figure S1. Due to the hexagonal geometry of the HPC system, the characteristic length given by the RDF intersections is actually the distance between cylinder rows ($\sqrt{3}$ in the Figure S1 inset) so d_{HPC} is calculated as the distance between the first and third crossings of $g_{AA}(r)$ and $g_{AB}(r)$ multiplied by a factor of $\frac{2\sqrt{3}}{3}$.[12]

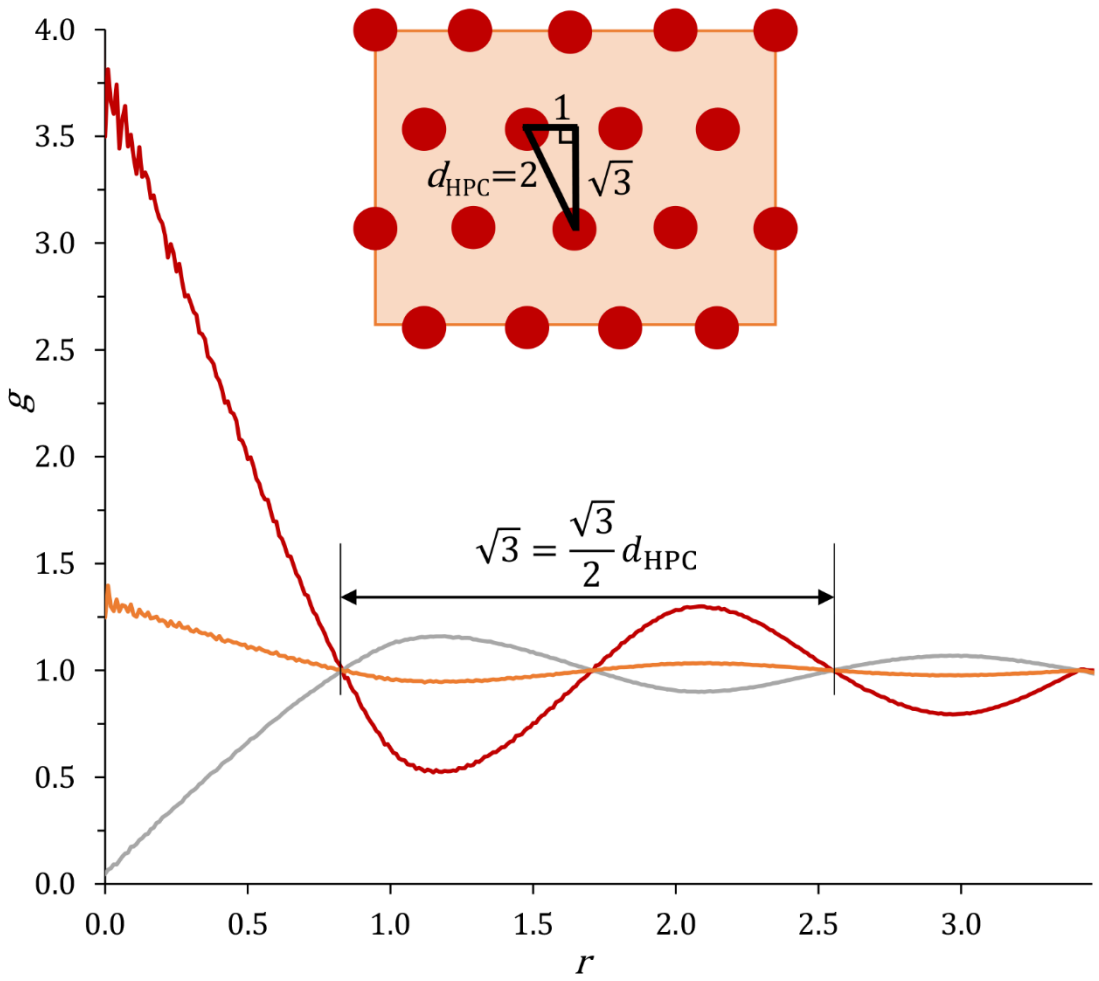

Figure S1. Radial distribution function measurement of domain spacing for the HPC structure shown in the inset. The distance between the first and third (or i and $i+2$) crossing points between $g_{AA}(r)$ (red trace), $g_{BB}(r)$ (orange) and $g_{AB}(r)$ (gray) gives the characteristic spacing between cylinder rows ($\sqrt{3}$ in this example). The hexagonal geometry of the system dictates that d_{HPC} (the inter-cylinder center-to-center spacing) is related to this characteristic length by a factor of $\frac{2\sqrt{3}}{3}$.

Section 3: Domain Spacing Measurements from Simulation

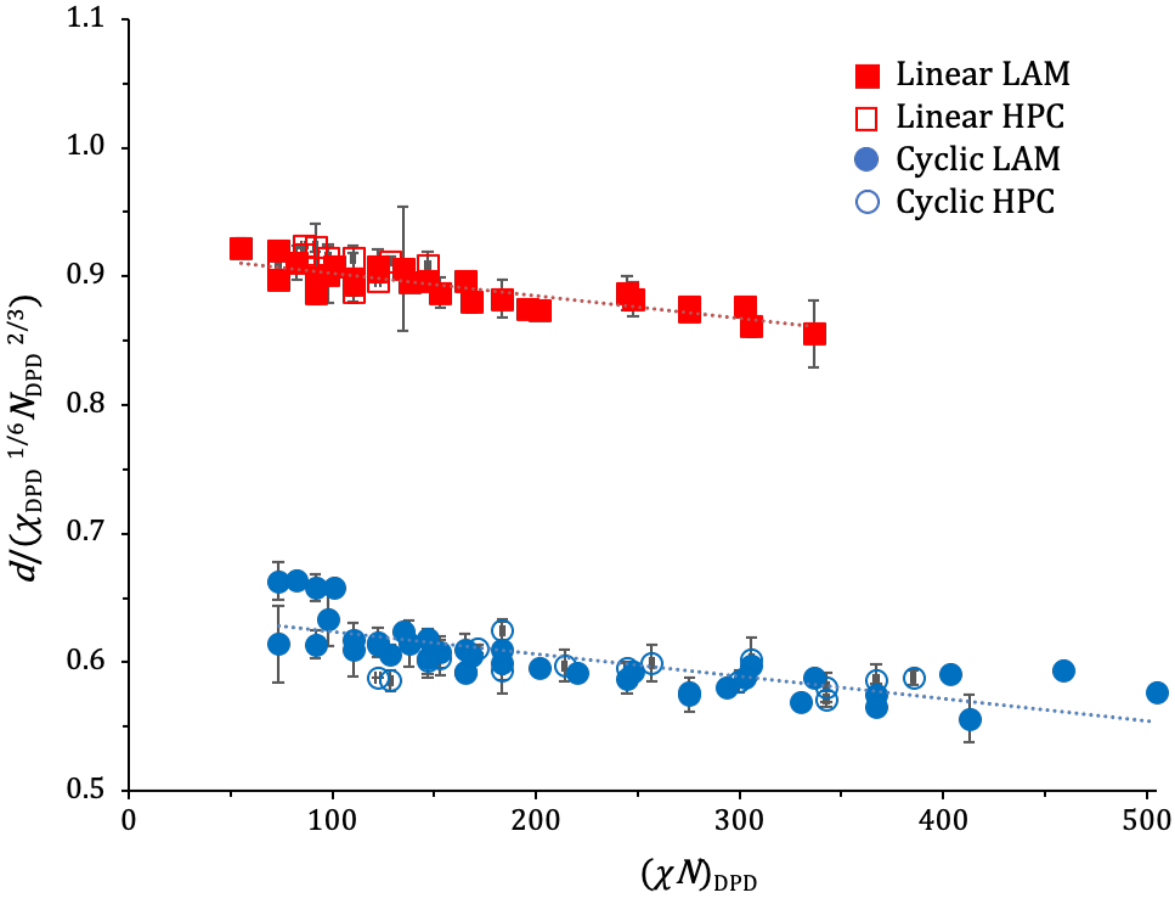

Figure S2. Ratio of domain spacings, d, measured from DPD simulation to the strong segregation theory (SST) scaling prediction, $\chi^{1/6}N^{2/3}$, as a function of segregation strength, χN. Lines are drawn to guide the eye. If the DPD simulations followed eq. (1), the simulated d would be a horizontal line at $d/(\chi^{1/6}N^{2/3}) = \beta$ for linear molecules and $d/(\chi^{1/6}N^{2/3}) = \beta/2^{2/3}$ for cyclic. The deviations observed here are due to the differences in the exponents calculated in this study (see Table 1, main text) and finite size effects. The smooth negative slope of the data points indicate that all simulated systems are strongly segregated; we do not observe any sharp changes in slope which would be associated with a scaling regime transition.

Table S1a: Cyclic lamellar BCP domain spacings

Architecture	*f*	*a*	χ	*N*	Trial	*d*
Cyclic	0.5	40	4.59	16	1	5.059
					2	5.066
					3	4.957
Cyclic	0.5	40	4.59	20	1	5.872
					2	5.859
					3	5.763
Cyclic	0.5	40	4.59	24	1	6.540
					2	6.540
					3	6.540
Cyclic	0.5	40	4.59	28	1	7.260
					2	7.268
					3	7.076
Cyclic	0.5	40	4.59	32	1	7.996
					2	7.996
					3	8.101
Cyclic	0.5	40	4.59	36	1	8.315
					2	8.624
					3	8.016
Cyclic	0.5	40	4.59	40	1	9.040
					2	9.040
					3	9.040
Cyclic	0.5	65	12.23	6	1	3.331
					2	3.331
					3	3.310
Cyclic	0.5	65	12.23	8	1	3.806
					2	3.890
					3	3.838
Cyclic	0.5	65	12.23	10	1	4.447
					2	4.284
					3	4.279
Cyclic	0.5	65	12.23	12	1	4.863
					2	4.682
					3	4.861
Cyclic	0.5	65	12.23	18	1	6.122
					2	6.390
					3	6.000
Cyclic	0.5	65	12.23	20	1	6.548
					2	6.540
					3	6.628
Cyclic	0.5	65	12.23	24	1	7.292
					2	7.420
					3	7.276
Cyclic	0.5	65	12.23	30	1	8.646
					2	8.315
					3	8.315
Cyclic	0.5	70	13.76	6	1	3.389
					2	3.393
					3	3.393
Cyclic	0.5	70	13.76	8	1	3.834
					2	3.838
					3	3.806
Cyclic	0.5	70	13.76	10	1	4.414
					2	4.414
					3	4.418
Cyclic	0.5	70	13.76	12	1	4.893
					2	4.893
					3	5.059
Cyclic	0.5	70	13.76	18	1	6.397
					2	6.122
					3	6.390

Architecture	*f*	*a*	χ	*N*	Trial	*d*
Cyclic	0.5	70	13.76	20	1	6.628
					2	6.548
					3	6.548
Cyclic	0.5	70	13.76	24	1	7.276
					2	7.460
					3	7.276
Cyclic	0.5	70	13.76	30	1	8.315
					2	8.315
					3	8.315
Cyclic	0.5	75	15.29	6	1	3.462
					2	3.417
					3	3.396
Cyclic	0.5	75	15.29	8	1	3.838
					2	3.838
					3	3.934
Cyclic	0.5	75	15.29	10	1	4.500
					2	4.418
					3	4.418
Cyclic	0.5	75	15.29	12	1	5.061
					2	5.061
					3	4.989
Cyclic	0.5	75	15.29	18	1	6.000
					2	6.540
					3	6.122
Cyclic	0.5	75	15.29	20	1	7.060
					2	6.876
					3	6.876
Cyclic	0.5	75	15.29	24	1	7.484
					2	7.276
					3	7.460
Cyclic	0.5	75	15.29	30	1	9.040
					2	9.030
					3	9.040
Cyclic	0.5	80	16.82	6	1	3.486
					2	3.462
					3	3.486
Cyclic	0.5	80	16.82	8	1	4.025
					2	3.970
					3	3.994
Cyclic	0.5	80	16.82	10	1	4.562
					2	4.466
					3	4.466
Cyclic	0.5	80	16.82	12	1	5.067
					2	4.863
					3	5.064
Cyclic	0.5	80	16.82	18	1	6.388
					2	6.396
					3	6.612
Cyclic	0.5	80	16.82	20	1	6.876
					2	7.068
					3	6.876
Cyclic	0.5	80	16.82	24	1	7.611
					2	8.005
					3	7.996
Cyclic	0.5	80	16.82	30	1	9.040
					2	8.656
					3	9.030

Table S1b: Linear lamellar BCP domain spacings

Architecture	*f*	*a*	χ	*N*	Trial	*d*
Linear	0.5	40	4.59	12	1	6.340
					2	5.994
					3	6.352
Linear	0.5	40	4.59	16	1	7.268
					2	7.316
					3	7.444
Linear	0.5	40	4.59	20	1	8.315
					2	8.315
					3	8.656
Linear	0.5	40	4.59	24	1	9.488
					2	9.787
					3	9.488
Linear	0.5	65	12.23	6	1	4.637
					2	4.568
					3	4.625
Linear	0.5	65	12.23	8	1	5.469
					2	5.474
					3	5.469
Linear	0.5	65	12.23	10	1	6.388
					2	6.394
					3	6.392
Linear	0.5	65	12.23	12	1	7.069
					2	7.267
					3	7.068
Linear	0.5	65	12.23	16	1	8.317
					2	8.659
					3	8.315
Linear	0.5	65	12.23	20	1	9.776
					2	9.992
					3	9.997
Linear	0.5	70	13.76	6	1	4.720
					2	4.568
					3	4.678
Linear	0.5	70	13.76	8	1	5.565
					2	5.565
					3	5.566
Linear	0.5	70	13.76	10	1	6.532
					2	6.388
					3	6.388
Linear	0.5	70	13.76	12	1	7.269
					2	7.268
					3	7.276

Architecture	*f*	*a*	χ	*N*	Trial	*d*
Linear	0.5	70	13.76	18	1	9.328
					2	9.328
					3	9.488
Linear	0.5	70	13.76	20	1	10.000
					2	9.883
					3	10.000
Linear	0.5	75	15.29	6	1	4.675
					2	4.675
					3	4.682
Linear	0.5	75	15.29	8	1	5.756
					2	5.564
					3	5.769
Linear	0.5	75	15.29	10	1	6.388
					2	6.540
					3	6.540
Linear	0.5	75	15.29	12	1	7.274
					2	7.274
					3	7.316
Linear	0.5	75	15.29	18	1	9.488
					2	9.485
					3	9.485
Linear	0.5	75	15.29	20	1	10.000
					2	9.997
					3	9.997
Linear	0.5	80	16.82	6	1	4.856
					2	4.850
					3	4.682
Linear	0.5	80	16.82	8	1	5.764
					2	5.764
					3	5.877
Linear	0.5	80	16.82	10	1	6.540
					2	6.542
					3	6.540
Linear	0.5	80	16.82	12	1	7.453
					2	7.272
					3	7.276
Linear	0.5	80	16.82	18	1	9.488
					2	9.488
					3	9.936
Linear	0.5	80	16.82	20	1	10.267
					2	10.000
					3	10.000

Table S1c: HPC domain spacings

Architecture	f	a	χ	N	Trial	d
Cyclic	0.25	35	3.06	40	1	
					2	
					3	8.288
Cyclic	0.25	40	4.59	28	1	6.884
					2	7.076
					3	6.928
Cyclic	0.25	40	4.59	32	1	7.866
					2	7.653
					3	7.919
Cyclic	0.25	40	4.59	36	1	8.365
					2	8.383
					3	8.248
Cyclic	0.25	40	4.59	40	1	8.993
					2	8.669
					3	9.215
Cyclic	0.25	50	7.65	20	1	6.248
					2	6.381
					3	6.099
Cyclic	0.25	60	10.70	16	1	5.716
					2	5.776
					3	5.773
Cyclic	0.25	60	10.70	20	1	6.396
					2	6.544
					3	6.662
Cyclic	0.25	60	10.70	24	1	7.209
					2	7.478
					3	7.531
Cyclic	0.25	60	10.70	28	1	8.124
					2	7.894
					3	8.019
Cyclic	0.25	60	10.70	32	1	8.494
					2	8.503
					3	8.660
Cyclic	0.25	60	10.70	36	1	8.197
					2	9.465
					3	9.623
Cyclic	0.25	65	12.23	28	1	8.143
					2	7.967
					3	8.283
Cyclic	0.25	75	15.29	12	1	5.187
					2	5.192
					3	5.094
Cyclic	0.25	75	15.29	16	1	5.997
					2	5.908
					3	5.973
Cyclic	0.25	75	15.29	20	1	6.884
					2	6.884
					3	7.217
Cyclic	0.25	75	15.29	24	1	7.847
					2	7.690
					3	7.531

Architecture	f	a	χ	N	Trial	d
Linear	0.25	35	3.06	24	1	9.071
					2	9.216
					3	9.085
Linear	0.25	35	3.06	28	1	10.263
					2	10.263
					3	10.255
Linear	0.25	40	4.59	20	1	8.631
					2	8.311
					3	8.660
Linear	0.25	40	4.59	24	1	9.481
					2	9.481
					3	9.619
Linear	0.25	50	7.65	12	1	6.851
					2	6.878
					3	6.638
Linear	0.25	50	7.65	16	1	
					2	
					3	7.986
Linear	0.25	60	10.70	8	1	5.457
					2	5.466
					3	5.412
Linear	0.25	60	10.70	12	1	7.074
					2	7.122
					3	7.092
Linear	0.25	65	12.23	8	1	5.495
					2	5.541
					3	5.623
Linear	0.25	65	12.23	12	1	7.329
					2	7.170
					3	7.187
Linear	0.25	70	13.76	8	1	5.650
					2	5.607
					3	5.724
Linear	0.25	75	15.29	8	1	5.792
					2	5.794
					3	5.773

Section 4: Derivation of σ from random walk statistics

The squared end-to-end length R_{ee}^2 of a linear molecule is proportional to the number of bonds in the molecule (which is one less than the number of monomers (N)), and the length of the bond between adjacent monomers, b_i

$$\langle R_{ee}^2 \rangle = \sum_{j=1}^{N-1} \sum_{i=1}^{N-1} \langle \overrightarrow{b_i} \cdot \overrightarrow{b_j} \rangle . \tag{S9}$$

In the case where bond length differences are negligible (the assumption underlying Semenov's Strong Segregation Theory, main text eq. (1)), we define

$$\langle R_{ee}^2 \rangle_0 = (N-1)b^2. \tag{S10}$$

For relatively short block copolymers, however, the interfacial bonds between unlike monomers, b_{AB}, measure ~35% longer than bonds between like monomers, b_{ii} (i = A or B), for both the linear and cyclic BCPs. Due to the highly coarse-grained (*i.e.*, very short) chains used in DPD simulation, the localized interfacial stretching contributes significantly to the effective polymer length. In this situation, the squared end-to-end length of a linear BCP becomes

$$\langle R_{ee}^2 \rangle = (N-2)b_{AA}^2 + b_{AB}^2. \tag{S11}$$

Multiplying and dividing by $(N-1)$ and factoring out b_{AA} gives

$$\langle R_{ee}^2 \rangle = \frac{b_{AA}^2 \left[N-1+\left(\frac{b_{AB}}{b_{AA}}\right)^2 - 1 \right]}{N-1} (N-1), \tag{S12}$$

so that the ratio of mean squared end-to-end length for a BCP with significant interfacial stretching to that of an unstretched molecule is

$$\frac{\langle R_{ee}^2 \rangle}{\langle R_{ee}^2 \rangle_0} = \frac{N-1+\left(\frac{b_{AB}}{b_{AA}}\right)^2 - 1}{N-1} = 1 + \frac{1}{\lambda_{\text{lin}}} \left[\left(\frac{b_{AB}}{b_{AA}}\right)^2 - 1 \right] \tag{S13}$$

where $\lambda_{\text{lin}} = N-1$. This ratio can be considered a correction for the interfacial chain elongation observed in strongly-segregated BCPs. We therefore include it as part of Λ, the term representing polymer size in eq. (4), defining,

$$\sigma = 1 + \frac{1}{\lambda}\left[\left(\frac{b_{AB}}{b_{AA}}\right)^2 - 1\right], \tag{S14}$$

and

$$\Lambda = \lambda\sigma = \lambda + \left(\frac{b_{AB}}{b_{AA}}\right)^2 - 1. \tag{S15}$$

Table S2 gives values for the ratio b_{AB}/b_{AA} measured in simulations of cyclic and linear BCPs over a range of chain lengths, morphologies, and architectures. An average value of 1.356 was used for eq. (4) fitting.

Table S2: Values of the ratio b_{AB}/b_{AA} measured in DPD simulation

Architecture	*f*	*a*	χ	*N*	b_{AB}/b_{AA}
Cyclic	0.5	40	4.6	16	1.200
Cyclic	0.5	40	4.6	20	1.192
Cyclic	0.5	40	4.6	24	1.187
Cyclic	0.5	40	4.6	28	1.183
Cyclic	0.5	65	12.2	6	1.464
Cyclic	0.5	65	12.2	10	1.370
Cyclic	0.5	65	12.2	12	1.350
Cyclic	0.5	65	12.2	20	1.317
Cyclic	0.5	65	12.2	30	1.301
Cyclic	0.5	80	16.8	6	1.521
Cyclic	0.5	80	16.8	10	1.412
Cyclic	0.5	80	16.8	12	1.391
Cyclic	0.5	80	16.8	20	1.356
Cyclic	0.5	80	16.8	30	1.340
Cyclic	0.25	40	4.6	28	1.183
Cyclic	0.25	40	4.6	32	1.180
Cyclic	0.25	40	4.6	36	1.178
Cyclic	0.25	40	4.6	40	1.176
Cyclic	0.25	65	12.2	28	1.307
Linear	0.5	40	4.6	12	1.196
Linear	0.5	40	4.6	16	1.187
Linear	0.5	40	4.6	20	1.180
Linear	0.5	40	4.6	24	1.177
Linear	0.5	65	12.2	6	1.369
Linear	0.5	65	12.2	10	1.328
Linear	0.5	65	12.2	12	1.318
Linear	0.5	65	12.2	20	1.301
Linear	0.5	80	16.8	6	1.409
Linear	0.5	80	16.8	10	1.367
Linear	0.5	80	16.8	12	1.356
Linear	0.5	80	16.8	20	1.338
Linear	0.25	40	4.6	20	1.183
Linear	0.25	40	4.6	24	1.178
Linear	0.25	65	12.2	8	1.351
Linear	0.25	65	12.2	12	1.326

To confirm the validity of using random walk statistics to describe BCPs in DPD simulation, we calculated the g-factor ($R^2_{g,cyc}/R^2_{g,lin}$) for $6 \leq N_{DPD} \leq 20$ at $\chi = 12.2$ and $\chi = 15.3$. We found $0.46 < R^2_{g,cyc}/R^2_{g,lin} < 0.53$, in good agreement with the random walk theory prediction of 0.50. This narrow range suggests that our use of random walk principles in developing the revised scaling law is reasonable.

Table S3: Radii of gyration (R_g) for cyclic and linear BCPs of identical N_{DPD}. Standard deviations for all R_g measurements are less than 0.005.

χ	N	$R_{g,cyc}$	$R_{g,lin}$	$(R_{g,cyc}/ R_{g,lin})^2$
12.2	6	0.651	0.896	0.528
12.2	8	0.762	1.068	0.509
12.2	10	0.873	1.229	0.505
12.2	12	0.966	1.366	0.500
12.2	20	1.29	1.874	0.474
15.3	6	0.660	0.905	0.532
15.3	8	0.767	1.09	0.495
15.3	10	0.880	1.24	0.504
15.3	12	0.981	1.39	0.498
15.3	18	1.21	1.78	0.462
15.3	20	1.34	1.88	0.508

Section 5: Predicting percent reduction in lamellar size from cyclization

The percent reduction in lamellar size that can be achieved by cyclizing a linear BCP of length N is defined as

$$\%\, reduction = (d_{lin} - d_{cyc})/d_{lin} \times 100\%, \tag{S16}$$

which can be calculated from eq. (4) as

$$\%\, reduction = \frac{(\beta\Lambda^{\varepsilon}\chi^{\gamma})_{lin} - (\beta\Lambda^{\varepsilon}\chi^{\gamma})_{cyc}}{(\beta\Lambda^{\varepsilon}\chi^{\gamma})_{lin}} \times 100\%. \tag{S17}$$

Because the cyclic product will have the same f and χ as its linear precursor, the β and χ terms cancel to give

$$\%\, reduction = \frac{(\Lambda^{\varepsilon})_{lin} - (\Lambda^{\varepsilon})_{cyc}}{(\Lambda^{\varepsilon})_{lin}} \times 100\%. \tag{S18}$$

Plugging the definition of Λ into the equation gives

$$\%\, reduction = \frac{\left[\mathrm{N}-1+\left(\frac{b_{AB}}{b_{AA}}\right)^2-1\right]^{\varepsilon} - \left[\frac{\mathrm{N}}{2}+\left(\frac{b_{AB}}{b_{AA}}\right)^2-1\right]^{\varepsilon}}{\left[\mathrm{N}-1+\left(\frac{b_{AB}}{b_{AA}}\right)^2-1\right]^{\varepsilon}} \times 100\% \tag{S19}$$

which simplifies to

$$\%\, reduction = \left(1 - \frac{\left[\frac{\mathrm{N}}{2}+\left(\frac{b_{AB}}{b_{AA}}\right)^2-1\right]^{\varepsilon}}{\left[\mathrm{N}+\left(\frac{b_{AB}}{b_{AA}}\right)^2-2\right]^{\varepsilon}}\right) \times 100\%. \tag{S20}$$

The lines in Figure 5 come from this equation. In the long chain limit, the % reduction plateaus based on the scaling exponent as

$$\lim_{N\to\infty}(\%\, reduction) = \left(1 - \left[\frac{1}{2}\right]^{\varepsilon}\right) \times 100\%. \tag{S21}$$

We achieve this same limiting result by starting with eq. (1) (Semenov's Strong Segregation Theory) and applying Marko's hypothesis that a cyclic BCP should scale $(N/2)^{2/3}$ in the long chain limit. In this approach, the β and χ terms cancel to give

$$\%\, reduction = \frac{N^{2/3} - \left(\frac{N}{2}\right)^{2/3}}{N^{2/3}} \times 100\%. \tag{S22}$$

which simplifies to

$$\%\, reduction = \left(1 - \left[\frac{1}{2}\right]^{2/3}\right) \times 100\% = 37\%. \tag{S23}$$

References

1. Groot, R. D.; Madden, T. J. Dynamic simulation of diblock copolymer microphase separation. *The Journal of Chemical Physics* **1998,** 108 (20), 8713-8724.

2. Qian, H.-J.; Lu, Z.-Y.; Chen, L.-J.; Li, Z.-S.; Sun, C.-C. Computer Simulation of Cyclic Block Copolymer Microphase Separation. *Macromolecules* **2005,** 38 (4), 1395-1401.

3. Gavrilov, A. A.; Kudryavtsev, Y. V.; Chertovich, A. V. Phase diagrams of block copolymer melts by dissipative particle dynamics simulations. *The Journal of Chemical Physics* **2013,** 139 (22), 224901.

4. Posel, Z.; Lísal, M.; Brennan, J. K. Interplay between microscopic and macroscopic phase separations in ternary polymer melts: Insight from mesoscale modelling. *Fluid Phase Equilibria* **2009,** 283 (1), 38-48.

5. Soto-Figueroa, C.; Rodríguez-Hidalgo, M.-d.-R.; Martínez-Magadán, J.-M.; Vicente, L. Dissipative Particle Dynamics Study of Order−Order Phase Transition of BCC, HPC, OBDD, and LAM Structures of the Poly(styrene)−Poly(isoprene) Diblock Copolymer. *Macromolecules* **2008,** 41 (9), 3297-3304.

6. Groot, R. D.; Warren, P. B. Dissipative particle dynamics: Bridging the gap between atomistic and mesoscopic simulation. *The Journal of Chemical Physics* **1997,** 107 (11), 4423-4435.

7. Groot, R. D.; Madden, T. J.; Tildesley, D. J. On the role of hydrodynamic interactions in block copolymer microphase separation. *The Journal of Chemical Physics* **1999,** 110 (19), 9739-9749.

8. Nikunen, P.; Vattulainen, I.; Karttunen, M. Reptational dynamics in dissipative particle dynamics simulations of polymer melts. *Physical Review E* **2007,** 75 (3), 036713.

9. Allen, M. P.; Tildesley, D. J., *Computer Simulation in Chemical Physics*. Springer Science & Business Media: 2012; Vol. 397.

10. Espanol, P.; Warren, P. Statistical mechanics of dissipative particle dynamics. *EPL (Europhysics Letters)* **1995,** 30 (4), 191.

11. Jiao, G.-S.; Li, Y.; Qian, H.-J.; Lu, Z.-Y. Computer simulation study of polydispersity effect on the phase behavior of short diblock copolymers. *Polymer* **2016**.

12. Tanaka, H.; Hasegawa, H.; Hashimoto, T. Ordered structure in mixtures of a block copolymer and homopolymers. 1. Solubilization of low molecular weight homopolymers. *Macromolecules* **1991,** 24 (1), 240-25.